IJE TRANSACTIONS B: Applications Vol. 37 No. 08, (August 2024) 1486-1499

International Journal of Engineering

Journal Homepage: www.ije.ir

Enhancing Low-Pass Filter Energy Management with Adaptive State of Charge Limiter for Hybrid Energy Storage in Electric Vehicles

H. Maghfiroh*[a,b], O. Wahyunggoro[a], A. Imam Cahyadi[a]

[a] *Department of Electrical and Information Engineering, Universitas Gadjah Mada, Yogyakarta, Indonesia*
[b] *Department of Electrical Engineering, Universitas Sebelas Maret, Surakarta, Indonesia*

PAPER INFO

Paper history:
Received 16 October 2023
Received in revised form 31 December 2023
Accepted 22 Januray 2024

Keywords:
Electric Vehicle
Hybrid Sources
Energy Management
Low-Pass Filter
Fuzzy Logic Controller

ABSTRACT

Electric vehicles (EVs) have become a vital solution for environmental transportation; however, challenges related to battery life and power density persist. In pursuit of enhanced EV performance and cost-effectiveness, researchers advocate for Hybrid Energy Storage Systems (HESS), integrating various Energy Storage Systems (ESS). An efficient Energy Management Strategy (EMS) is crucial for optimal power distribution within the HESS. This study introduces a real-time, simple, and practical EMS using a low-pass filter (LPF). However, the LPF lacks State of Charge (SoC) control, necessitating the addition of a SoC Limiter. The static SoC Limiter, while effective, faces challenges in predicting peak loads, leading to suboptimal power-sharing performance. To address this limitation, LPF with Adaptive SoC Limiter (LPF-ASL) is proposed. The LPF-ASL accommodates the peak load by saving some portion of supercapacitor (SC) power for peak load. In an unpredictable initial SC SoC test, LPF-ASL achieves substantial reductions in maximum battery current compared to LPF and Fuzzy Logic Control (FLC) by up to 21.30% and 21.14%, respectively. This underscores the effectiveness of LPF-ASL in optimizing battery life and enhancing power distribution within HESS-equipped EVs.

***doi**: 10.5829/ije.2024.37.08b.03*

Graphical Abstract

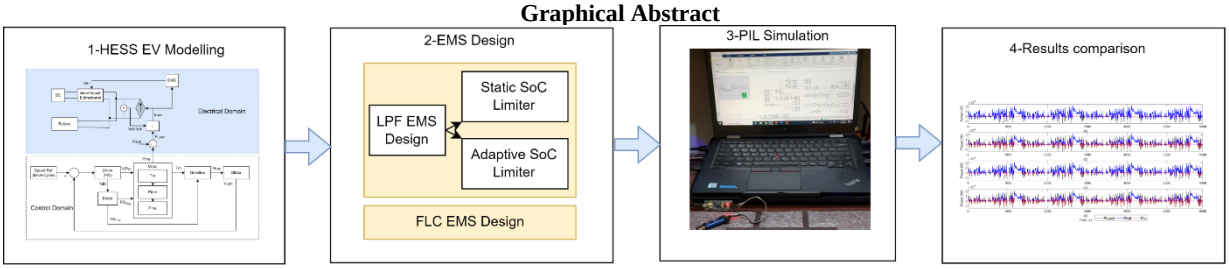

1. INTRODUCTION

Environmental problems from carbon dioxide emissions are serious and have a direct impact on climate changes (1). Therefore, the need for eco-friendly transportation is rising, and electric vehicles (EVs) have become a popular alternative to vehicles powered by internal combustion engines. According to Ihsan et al. (2), many countries in the world have promoted the development of the use of EVs to overcome the problems of the energy crisis and global warming. However, EVs still have problems to solve, one of them is regarding the battery life and its power density (3). Therefore, researchers have combined different Energy Storage Systems (ESS) to create hybrid-ESS (HESS), which may suit driving needs, and improve the battery lifetime and performance of the vehicle.

*Corresponding Author Email: hari.maghfiroh@gmail.com
(H. Maghfiroh)

Please cite this article as: Maghfiroh H, Wahyunggoro O, Imam Cahyadi A. Enhancing Low-Pass Filter Energy Management with Adaptive State of Charge Limiter for Hybrid Energy Storage in Electric Vehicles. International Journal of Engineering, Transactions B: Applications. 2024;37(08):1486-99.

Long-term cost-effectiveness for EVs can be achieved by extending the battery's life as it is one of the most expensive parts of an EV. According to Gunther et al. (4), the HESS can increase efficiency and minimize costs while enhancing overall system performance. Based on Hemmati and Saboori (5) the battery-supercapacitor HESS is the most promising arrangement for EV applications. The HESS concept is also applied in the power system which accommodates many power sources as reported in literature (6, 7).

The HESS needs an Energy Management Strategy (EMS) to properly distribute the power usage of the ESSs (8). According to Tran et al. (9) and Gautam et al. (10), the objective of EMS has to satisfy the limitation, utilizes ESS effectively, improves comfort and drivability, increases fuel economy, and reduces emissions. EMS techniques are divided into three groups: rule-based, optimization-based, and learning-based (11, 12). According to literature (8, 13, 14), the rule-based method is accurate and has a short computation time, allowing it to be employed in real-time. This strategy is used by the Toyota Prius and Honda Insight (15).

In this work, the low-pass filter (LPF) technique, a component of rule-based EMS, is applied since it is the simplest and most used approach, according to Asensio et al. (16). Moreover, based on literature (17-19), it is simple, has dependable performance, and offers good dynamics and cycle reduction. The working principle of LPF as EMS is to decouple the low frequency from the load power and send it to the ESS with slower responses. In the case of the HESS battery-supercapacitor (SC), the battery has a slower response time than the SC. According to Traore et al. (20), the frequency domain EMS can lengthen battery life by tackling transient phenomena in power usage.

Finding the proper cut-off frequency is difficult when using LPF as an EMS. The Ragone plot, as used by Snoussi et al. (21) Maghfiroh et al. (22), is the typical technique for finding the cut-off frequency of LPF as EMS. Fast Fourier Transform (FFT) (23, 24), Power Spectral Density (PSD) (25), Numerical Calculation (26), and Trial (27) are additional techniques that many researchers have employed. Some studies employ optimization to determine the best cut-off frequency, as discussed by Huang et al. (28), El Aoumari and Oaudi (29), and the adaptive algorithms, as giben by Zhang et al. (30), Liao et al. (31), to enhance the performance of LPF EMS. The basic and simplest method for this investigation is the Ragone plot.

Studies conducted by Syahbana and Trilaksono (32) and Snoussi et al. (33) have demonstrated the validity of the Ragone plot. Three power sources—a fuel cell (FC), a battery (B), a supercapacitor (SC), and two low-pass filters (LPF)—are used (32). FC requires some of the power from the first LPF, while the remainder is transmitted to the second LPF, which outputs power for the battery. The remaining portion of the second LPF is forwarded to SC. The authors conclude that this technique can make use of the SC's strength during the transitory phase before moving on to the battery and FC, perhaps extending the lifetime of the ESS. Use the same power sources and various filters as discussed by Syahbana and Trilaksono (32) and Snoussi et al. (33). The analysis is expanded on the sizing of each power source. Only software simulation is used for the verification.

The LPF EMS lacks State of Charge (SoC) control. Therefore, SoC limiters need to be added to guarantee that the ESS works in a safe SoC range. The static SoC limiter cannot help the LPF to predict the peak load power. As a result, the SC power is already used in the high-load event not the peak load. When peak load comes, SC is already in the lower SoC limit and cannot contribute to reducing the peak power. LPF with Adaptive SoC Limiter (LPF-ASL) is proposed to solve this issue. The LPF-ASL uses a small portion of SC power in low load and saves some portion for peak load.

In this study, the specific goals are twofold. Firstly, to solve LPF EMS issues regarding the SoC limiter using an ASL approach. The primary objective of this energy management system is to minimize battery deterioration while ensuring efficient power distribution between the dual energy sources. Secondly, to evaluate and compare the performance of the LPF-ASL with conventional LPF and Fuzzy Logic Control (FLC) approach. To achieve this, a Processor in the Loop (PIL) simulation is implemented using cost-effective hardware. The study's contributions are: 1) improving the LPF EMS which lacks SoC control with Adaptive-SoC Limter(ASL), 2) providing a comprehensive comparison between LPF-ASL, LPF, and FLC as EMS in the PIL implementation using cost-effective hardware, and 3) accounting for the non-linearity effect, use the detailed model of ESS and switching DC-DC converter model.

The rest of the paper is organized as follows: section 2 reviews the electric vehicle model used including the simulation design, the proposed LPF EMS, and the FLC method as a comparative method. The testing results and discussion are in section 3. Finally, the conclusion is provided in section 4.

2. MATERIALS AND METHODS

The procedural sequence of this investigation is illustrated in Figure 1. It commences with the modeling of the Hybrid Energy Storage System (HESS) for Electric Vehicles, incorporating detailed representations of the Energy Storage System (ESS) and DC-DC converter to address non-linearities. Simultaneously, the design of the Low-Pass Filter Energy Management System (LPF EMS) is initiated alongside the Fuzzy Logic Control

Energy Management System (FLC EMS). Following this, the introduction of the proposed Adaptive State of Charge (SoC) Limiter into the LPF EMS takes place. Subsequently, a Processor in the Loop (PIL) simulation is executed. Ultimately, the results are compared and subjected to analysis.

2. 1. Materials In this investigation, a city car with the specs shown in Table 1 is employed. The information is borrowed, albeit much modified by Yi et al. (34). The mass of the DC/DC converter, SC, and battery is derived by Michalczuk et al. (35). In this study, a single DC-DC converter located on the semi-active supercapacitor's SC side was utilized. Cost and electrical transfer capacity are sacrificed in this system. Because the semi-active system only utilizes one DC-DC converter to control energy flow, it offers greater energy sharing than the passive alternative. On the other hand, the semi-active configuration is less costly and easier to operate than the active version, which uses DC-DC converters in every energy storage. The auxiliary load and the traction motor's propulsion load together make up the HESS load in this system. Auxiliary power is considered constant power, although the propulsion load is variable and regulated by the driver's foot on the gas pedal.

The block diagram for the simulation design is shown in Figure 2. The speed reference, in this case, is the typical drive cycle. The driver block receives this signal and decides whether to accelerate or brake based on the speed references. This block consists of a PID control that replaces the driver and handles the velocity difference between reference and measured speeds (v_{veh}). Positive output from the driver is denoted by the symbol *%Pwr*, which stands for the percentage of throttle (100% *Pwr* represents full throttle). While the *%Br* stands for the driver's negative output and refers to the driver's percentage of braking. The brake signal (*%Br*) is separated into the friction (FB_{Fric}) and regenerative (FB_{Reg}) brake portions in the braking block, as depicted in Equations 1 and 2, respectively. Whereas FB_{max} and *RegenPortion* are the maximum braking force and regenerative braking portion with the value of 1,797 N and 1, respectively. The friction brake will be activated at a low speed when regenerative braking has a low impact. In this design, it will be active at a speed < 8 km/h. The motor performs regenerative braking; therefore, this signal is forwarded to the motor block. The motor torque (T_m) is determined by Equation 3, while the mechanical power (P_{mm}) of the motor is determined by Equation 4. Where T_{m_max} is the maximum torque of the motor. The traction motor's electric power (P_{me}) is calculated using Equation 5, and auxiliary power (P_{aux}) is then supplied to the EMS for power sharing with the battery and supercapacitor system.

The procedures in the driveline block use the torque signal from the motor to calculate the traction force (F_{trac}) based on Equation 6. T_{sloss}, on the other hand, is the

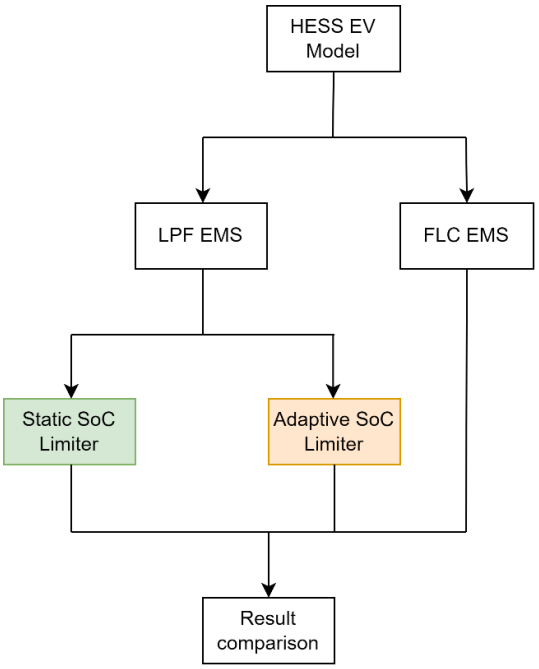

Figure 1. Research flow process

TABLE 1. EV model parameters and its HESS

Parameters	Value	Unit
Vehicle mass without ESS	515	kg
Driver mass	75	kg
Traction motor power (P_{m_max})	30	kW
Traction motor torque (T_{m_max})	110	Nm
Traction motor efficiency (η)	0.88	-
Windward area (Af)	2.04	m2
Rolling resistance coefficient (c_{roll})	0.0112	-
Air resistance coefficient (Cd)	0.25	-
Wheel radius (r_w)	0.252	m
Transmission ratio (G)	3.515	-
Auxiliary load (P_{aux})	0	W
Energy Storage System Parameters		
Battery rated capacity (Q_B)	150	Ah
Battery rated voltage (V_B)	115	V
Battery c-rate of charging and discharging	0.5c and 1c	-
Battery mass	200	kg
SC module-rated capacity (C_{SC})	33	F
SC module-rated voltage (V_{SC})	94.5	V
SC&DC/DC converter mass	10	kg

propulsion system's spin loss, in this test with a constant value of 6 Nm. Equation 7 is used by the Glider block to calculate the vehicle's acceleration and speed. This is based on Newton's law of motion, which considers the force acting on the moving object. M_{veh} stands for vehicle effective mass which is a combination of all mass for measurement including vehicle, driver, and ESS mass. Equations show how to calculate formulas for wheel friction (F_{roll}), air friction (F_{aero}), and gravitational force (F_{grade}), correspondingly (8–10) (36). Where Af is the vehicle's cross-sectional area, Cd is its drag coefficient, g is its gravitational acceleration, δ is the angle of inclination of the road, and c_{roll} is its rolling resistance coefficient, ρ_{Air} is the air density, which is normally 1.25 kg/m^3. Some of the variables and its value are already listed in Table 1.

$$FB_{Reg} = \%Br * FB_{max} * RegenPortion \quad (1)$$

$$FB_{Fric} = FB_{max} - FB_{Reg} \quad (2)$$

$$T_m = \left(\%Pwr * T_{m\_max}\right) + (FB_{Reg} * r_w/G) \quad (3)$$

$$P_{mm} = T_m(v_{veh}G/r_w) \quad (4)$$

$$P_{me} = P_{mm}/\mu \quad (5)$$

$$F_{trac} = ((T_m - T_{sloss}) * G \div r_w) - FB_{Fric} \quad (6)$$

$$\frac{dv_{veh}}{dt} = (F_{trac} - F_{roll} - F_{aero} - F_{grade}) \div M_{veh} \quad (7)$$

$$F_{roll} = c_{roll}M_{veh}g\ cos\ (\delta) \quad (8)$$

$$F_{aero} = \frac{1}{2}\rho_{air}A_f C_d v_{veh}^2 \quad (9)$$

$$F_{grade} = M_{veh}g \sin(\delta) \quad (10)$$

A lithium-ion (Li-ion) battery is used, and the model makes use of the Generic Battery Model (GBM) in the MATLAB software. The model proposed by Tremblay and Dessaint (37) and experimentally validated over the 20–100% State of Charge (SoC) range on Li-ion batteries with good accuracy (5% inaccuracy). The battery is also built with a controlled voltage source and internal resistance. For a thorough description of the battery model equation referred to Tremblay and Dessaint (37).

The supercapacitor model is with the non-linear Stern-Tofel model discussed by Miniguano et al. (38). The Helmholtz capacitance (C_H) and the Gouy-Chapman capacitance (C_{GC}) make up the supercapacitor's total capacitance in the Stern-Tofel model (C_T). The supercapacitor equation model is also illustrated by Miniguano et al. (38) for further detail. The DC-DC Buck/Boost Bidirectional converter used in this work has a switching paradigm with inbuilt PID control. With the present reference *Isc**, it has current control. The current can only flow up to ±100A, non-linearity and losses can be considered by using the switching model of the DC-DC converter.

2. 2. Methods Energy management strategy (EMS) is important for HESS. There are various EMS methods. However, not all of them can be implemented in the real world due to high computational processes. In this study, LPF-ASL is proposed. Its performance is compared with

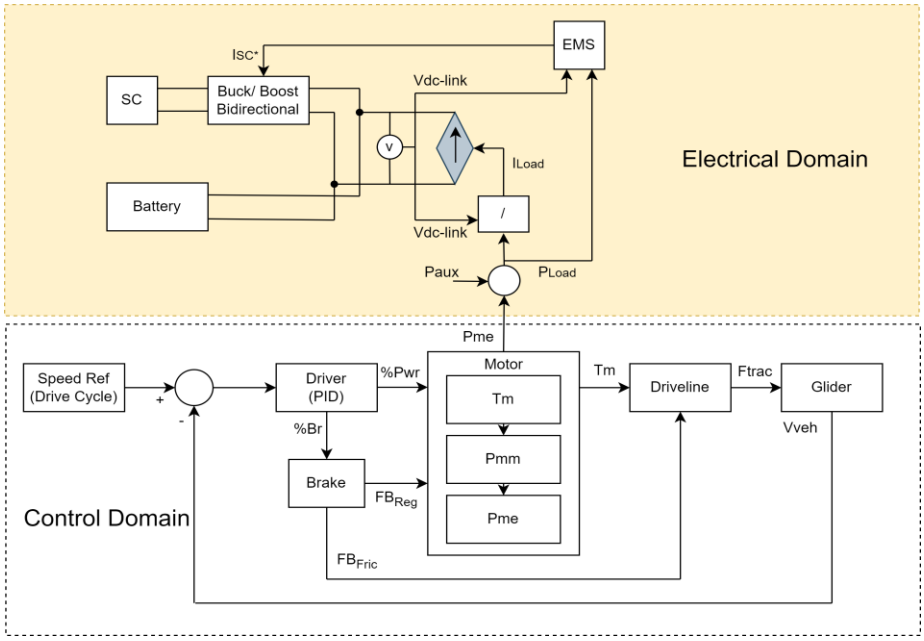

Figure 2. Block diagram of the simulation design

LPF and FLC methods. The PIL implementation using low-cost hardware is used to prove the real-time capability of these methods.

2. 2. 1. Low-Pass Filter (LPF) The working principle of LPF as EMS is to decouple the low frequency from the load power and send it to the battery. Whereas the rest with higher frequency is sent to SC. The challenge in the application of LPF as EMS is finding the right cut-off frequency. In this study, the Ragone plot method is chosen since it is simple and track-dependent.

The Ragone plot is a plot that shows the relation between power density and energy density of an energy storage system (ESS). Figure 3 shows a Ragone plot of some ESS. It is seen that the battery has high energy density with low power density. On the other hand, the supercapacitor has a low energy density with a high power density. From this plot, the cut-off frequency is calculated using Equation 11 (21). Where *fc*, ρ_{power}, and, ρ_{energy} are the cut-off frequency, power density, and energy density, respectively. Based on the Ragone plot in Figure 3, the cut of frequency can be chosen at any point in the battery area. Several tests were conducted at the edge of the battery rectangle area, and the cut-off frequency at (10^2, 10^4) which is 0.01 Hz, gave the best results.

$$f_c = \frac{\rho_{power}[W/kg]}{\rho_{energy}[J/kg]} \tag{11}$$

$$LPF = \frac{\omega}{s+\omega} \quad where \quad \omega = 2\pi f_c \tag{12}$$

Equation 12 is the first-order low-pass filter transfer function, where ω is the frequency in rad/s. To implement the LPF in the PIL, the continuous transfer function of the first-order LPF is transformed to the discrete form using the Tustin approximation or Bilinear transformation. The Bilinear transformation has the approximation relation between the S-domain and Z-domain as in Equation 13. Using this equation, step by step of Equations 14 to 18 are done to get the final discrete form LPF as in Equation 18. This equation is then translated into the Arduino code.

$$s = \frac{2}{T}\frac{1-z^{-1}}{1+z^{-1}} \tag{13}$$

$$\frac{V_{out}(z)}{V_{in}(z)} = \frac{\omega}{\frac{2}{T}\frac{1-z^{-1}}{1+z^{-1}}+\omega} \tag{14}$$

$$V_{out}(z) = \frac{\omega}{\frac{2}{T}\frac{1-z^{-1}}{1+z^{-1}}+\omega} V_{in}(z) \tag{15}$$

Both side times with T(1+z-1)

$$V_{out}(z)(2(1-z^{-1}) + \omega T(1+z^{-1})) = V_{in}(z)\omega T(1+z^{-1}) \tag{16}$$

$$V_{out(z)} = \frac{(2-\omega T)V_{out}(z)z^{-1}+\omega T V_{in}(z)+\omega T V_{in}(z)z^{-1}}{(2+\omega T)} \tag{17}$$

Since y(z) = x(z). z-1 then y(n)=x(n-1) therefore

$$V_{out}(n) = \frac{(2-\omega T)V_{out}(n-1)+\omega T V_{in}(n)+\omega T V_{in}(n-1)}{(2+\omega T)} \tag{18}$$

where V_{in}, V_{out}, T, and n are the input signal, output signal, sampling time, and sampling index, respectively.

Figure 4 is the structure of LPF as EMS. Load power(P_{Load}) is sent to the LPF which gives low-frequency power to the battery. Since the DC-DC converter used only one in the SC, the SC power reference is derived by subtracting the load power from the battery reference power from LPF. Since the LPF method cannot accommodate constrain, an SoC limiter is added to protect the SC in the safety SoC range. The SoC_{SC} is limited to 50-100%, to avoid SC being over-charged and over-discharged. According to Hussain et al. (39), the charge of SC is not allowed to go down below 50% of the maximum voltage. Since the DC-DC converter has current control; therefore, the power allocation for SC is divided by the DC-link voltage to get SC's current reference.

2. 2 .2. LPF with Adaptive SoC Limiter (LPF-ASL) The novel contribution of the proposed method is to combine LPF with the Adaptive SoC Limiter (ASL). In the conventional LPF EMS, a static SoC limiter is used to protect the SC from overcharging or overcharging. The

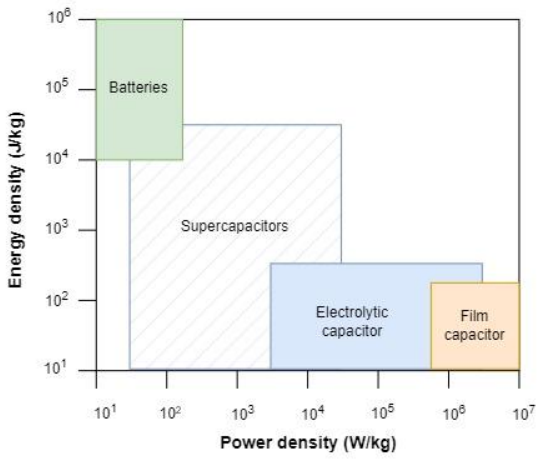

Figure 3. Ragone plot [24]

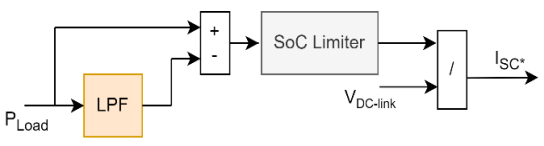

Figure 4. LPF EMS structure

weakness of this strategy is the power of SC can be used in the high load power event it is not the peak power. Therefore, at the peak power, the SC cannot give it power since it is already used and at the stage of lower SoC limit. In the proposed LPF-ASL, there are two stages of SC's SoC limit based on the battery current. When the battery current is low, the SC SoC range can be used is 70-100%. Whereas, if the battery current is high, the range of the SoC SC can be used is increased to 50-100%. The SoC limit is tuned manually in this study. Figure 5 shows the comparison of the static and adaptive SoC limiter in the flow diagram form. The blue block in Figure 5(b) is the adaptive mechanism. The battery current limit is determined as below the battery current specification which is 150 A. Therefore, 140 A is chosen. Too low current limit makes the SC used more frequently which reduces the capability to cut high load current. On the other hand, to high current limit will give a response that can over the limit. In the braking mode, there is no adaptive mechanism. When SC SoC is full 100%, the charge is stopped and the power from regenerative braking is sent to the battery.

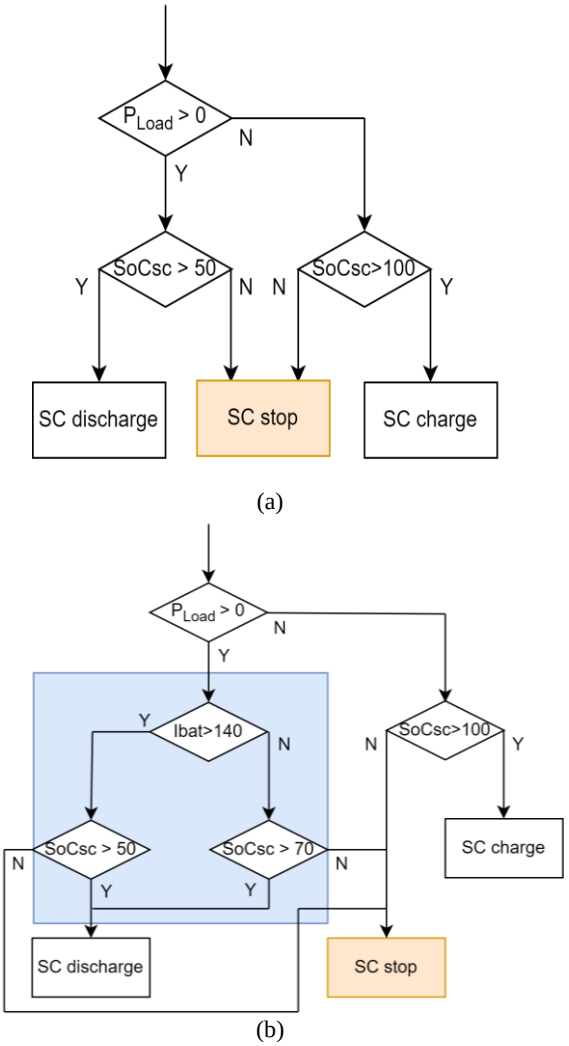

Figure 5. SoC Limiter: (a) static (b) adaptive

2. 2. 3. Fuzzy Logic Controller (FLC) Fuzzy Logic Controller (FLC) is part of artificial intelligence (AI) which uses a rule base that converts linguistic rules into control action (40). In the field of EMS, it can be used to distribute the power of the HESS based on the input and rules determined. The performance of FLC as EMS was already proven by Lin et al. (41) Najjaran et al. (42) Suhail et al. (43). FLC EMS is categorized into three main groups which are conventional, adaptive, and predictive (44-46). For this study, the conventional as the simple one is used.

The structure of the FLC EMS is illustrated in Figure 6 which uses Mamdani type fuzzy. The input of FLC is load power and SC SoC and the output is the scaling factor of SC's power. The output of FLC is then multiplied by load power to get the power reference for SC. The SoC limiter was also added to double protect the SC SoC in the permitted range.

Table 2 shows the fuzzy rules which are chosen manually. The membership functions of S, M, and B stand for Small, Medium, and Big, respectively. The principle to create the rules is, SC power allocation linear with load power and SoC_{SC}. For example, the higher the load power, the SC contributes more power. However, it is still limited with its SoC; therefore, in the small value of SoC, the power contribution is increased based on the load power starting from a small value. Whereas in the high SoC, it starts from a medium value. The number of rules is nine. The higher number of rules will make processing time increase. The defuzzification method used is the center of area (CoA).

Figure 7 shows the membership of FLC input and output which use the triangle function. The range of power value is chosen based on the maximum power absorbed in the battery-only mode. The range of SC's SoC is based on the optimal operating range of SC which is 50-100% of SoC. Whereas, the maximum scaling factor is chosen to be 0.3 which is the maximum power of SC (10kW) divided by the maximum power of the traction motor (30kW). This FLC system is only used when acceleration. In the braking mode, the negative power from regenerative braking is sent directly to the

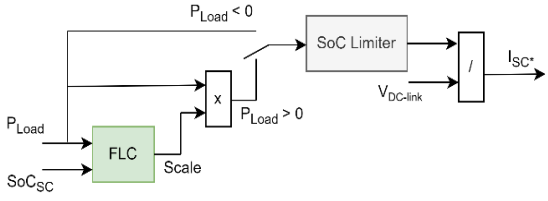

Figure 6. FLC EMS structure

TABLE 2. Fuzzy rules

SoCsc | Pdem	S	M	B
S	S	M	M
M	M	M	B
B	M	B	B

HESS. This power is used to charge the SC, when the SC SoC is full, the SoC protection will cut this power flow.

2. 2. 4. Performance Parameters Four factors—battery delta-SoC(ΔSoC_B), energy consumption, maximum battery current (Max I_B), and Battery Current Root Means Square (BCRMS)—are used to compare performance. The lower value is preferable in all terms. The battery peak current and BCRMS are the primary criteria in this study because the main goal is to increase battery lifetime. The battery delta-SoC is determined by subtracting the initial from the final SoC. The energy consumption is calculated using Equation 19. Where V_B and Q_B are the rated voltage and capacity of the battery, respectively. Whereas C_{SC} and V_{SC} are rated capacitance and voltage of the SC, respectively. The traveled distance in km is d. In the battery-only system, the SC energy is none. The BCRMS formula is shown in Equation 20, where Tf is the simulation time.

$$Energy\ Consumption(kWh/km) = \left(\Delta SoC_B(\%) * (V_B * Q_B)\right) + \left(\Delta SoC_{SC}(\%) * (0.5 * C_{SC} * V_{SC}^2)\right)\Big/_d \quad (19)$$

$$BCRMS = \sqrt{\frac{1}{T_f}\sum_{t=0}^{Tf} I_B^2} \quad (20)$$

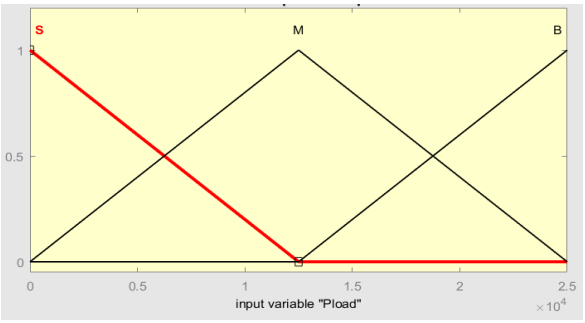

(a)

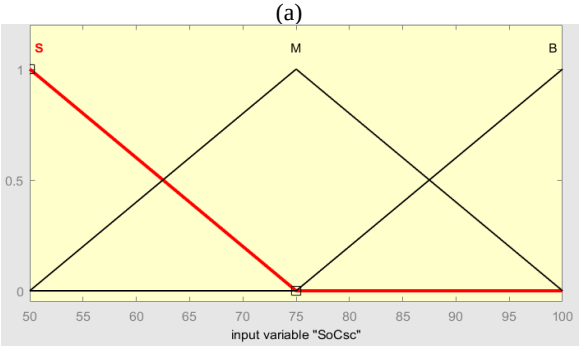

(b)

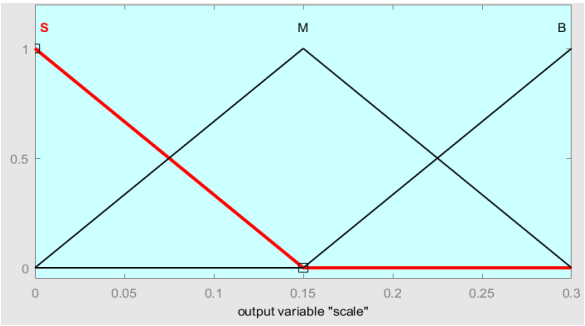

(c)

Figure 7. Fuzzy membership: (a) input P_{Load} (b) input SC's SoC, (c) output scaling

3. RESULTS AND DISCUSSION

The Worldwide Harmonized Light Vehicles Test Cycle (WLTC), a component of the Worldwide Harmonized Light Vehicles Test Procedure (WLTP), is the drive cycle utilized in this PIL test. The level of pollutants, CO_2 emissions, and fuel consumption of conventional, hybrid, and fully electric vehicles are all measured according to the WLTP global standard. Based on the vehicle's power-to-mass ratio (PMR) which is rated power (W) divided by vehicle mass (kg), there are three different WLTC classes, as resumed in Table 3. WLTC class 3 is used since the investigated vehicle model in this study is a class 3 vehicle. Because the vehicle type is designed for a top speed of 100 km/h, WLTC class 3a is used. There are four different speed levels: low, medium, high, and extra-high. Since the maximum speed of the extra-high phase is more than 100 km/h, only the low, medium, and high-speed phases are used. The low, medium, and high-speed phases have a distance of 3,095 m, 4,756 m, and 7,162 m, respectively. The test is conducted in both the individual and combined phases to verify the recommended approach. Consequently, the adaptability of the suggested strategy can be assessed. The gradient of the track is 0% or zero elevation.

The speed and power profiles of the WLTC driving cycles used are depicted in Figures 8(a) and 8(b), respectively. The power profile shown is calculated from the HESS configuration. To assess the improvement of the suggested method, the performance of the battery-only version is also compared. The battery-only system

TABLE 3. WLTC test cycle class (47)

Category	PMR (W/kg)	Speed max (km/h)
Class 1	PMR ≤ 22	-
Class 2	22 < PMR ≤ 34	-
Class 3a	PMR > 34	< 120
Class 3b	PMR > 34	≥ 120

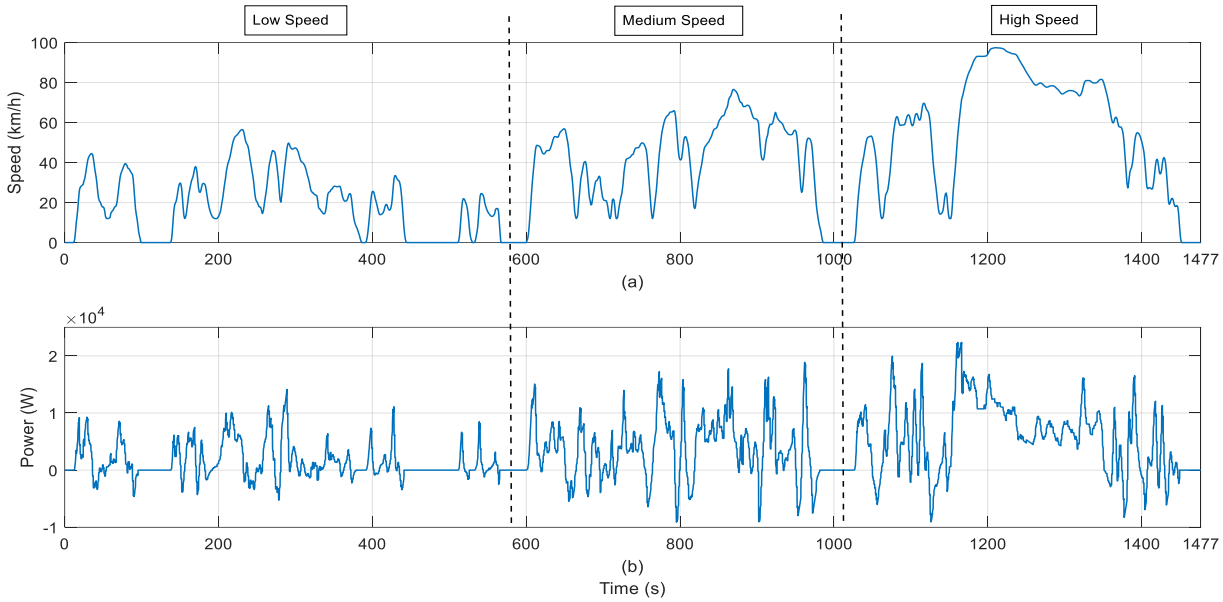

Figure 8. WLTP Class 3a: (a) speed; (b) power

has the same specification as the HESS EV except the weight of the SC and DC/DC converter is excluded. The battery and supercapacitor SoC are both set to 95% in the start condition.

3. 1. Processor in the Loop (PIL) Implementations

The processor used in the PIL implementation is a low-cost STM32F103C8T6 with a price of about US $6 on ebay.com. This small microcontroller has an ARM Cortex-M3 core that runs at 72MHz max. The code used is Arduino code and written in Arduino IDE. The LPF method only takes up 38% of the storage space. On the other side, the FLC takes 45% of the total storage space. This shows that the proposed method is simple and light.

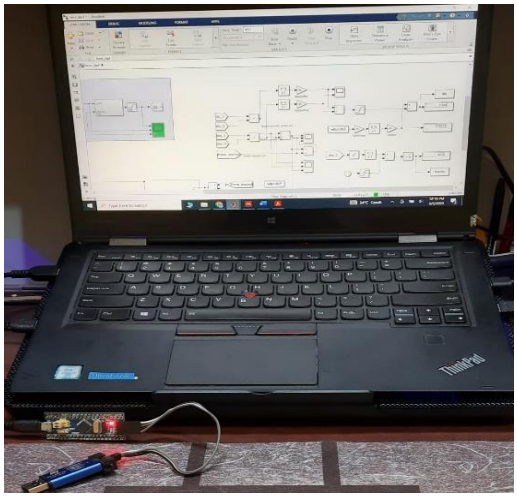

(a)

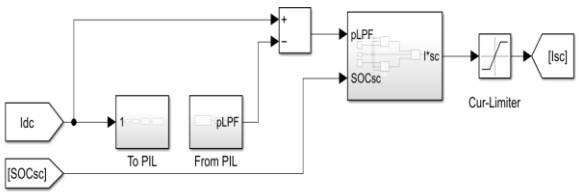

(b)

Figure 9. PIL configuration: (a) EV model in MATLAB Simulink connected to microcontroller through serial communication, (b) Simulink setup for PIL

Figure 9(a) shows the System model in MATLAB which is connected to STM32F103C8T6 via a USB port for serial communication. Whereas to download the code ST-LINK V2 is used. Figure 9(b) is the MATLAB Simulink block that accommodates this PIL simulation. The "To PIL" block is used to send the data to the microprocessor, whereas the "From PIL" block is to receive data from the microprocessor.

3. 2. Performance Analysis

In this part, the performance analysis for different drive cycle phases of WLTC is discussed. The purpose of this part is to know the performance and the robustness of the EMS method in the different speed ranges. The performance of LPF, FLC, LPF-ASL, and battery-only vehicles is compared and resumed for low-speed, medium-speed, high-speed, all-speed, and long-distance ranges as resumed in Tables 4-8, respectively.

The performance of the low-speed phase is resumed in Table 4. It shows that battery-only has the lowest value

of delta-SoC_B and energy consumption. Whereas in the HESS, LPF and LPF-ASL have nearly the same performance. FLC EMS has lower energy consumption than LPF and LPF-ASL but with higher peak current and BCRMS. In the medium-speed phase, Table 5, the HESS gives more impact at higher speeds. The HESS has a lower value in all criteria used. The delta-SoC_B of LPF is the lowest one. In energy consumption, all methods in HESS have the same value. In terms of maximum battery current, LPF has the lowest value. The proposed LPF-ASL has a higher peak current than the two other methods, but its value is still under the battery limit current which is 150 Ah (1 c-rate). In the BCRMS, LPF leads with the lowest value.

The high-speed performance gives different results, as shown in Table 6. The higher the speed, the advantages of the HESS give more impact. Compared to other EMS methods in HESS, FLC has lower delta-SoC_B and energy consumption. LPF has a lower delta-SoC_B than LPF-ASL with the same energy consumption. In the criteria of maximum battery current and BCRMS, LPF still leads with the lowest value followed by LPF-ASL. The proposed LPF-ASL has a higher value of maximum battery current and BCRMS due to it only using 70-100% SoC when the battery current is below 140 A. On the other hand, the LPF uses a wider SoC range which is 50-100%.

The next test is for all speed phases and long distances (4 times of all phases) with distances of 15,013 m (15 km) and 60, 052 m (60 km) tested, and the results are resumed in Tables 7 and 8, respectively. Table 7 shows that in the mixed-speed phase, FLC has the lowest delta-SoC_B and energy consumption. Whereas the energy consumption of LPF and LPF-ASL is the same, with lower delta-SoC_B for LPF. Battery-only system has the highest value of delta-SoC_B and energy consumption. In terms of maximum battery current and BCRMS, the LPF method still leads with the lowest value. The long-distance test result is shown in Table 8. In this test, the proposed LPF-ASL proved its performance with the lowest value on the maximum battery current and BCRMS. The maximum current reduction is up to 21.30%, and 21.14% compared to LPF and FLC EMS. Whereas in terms of delta-SoC_B and energy consumption is the same as the LPF method. FLC has the lowest delta-SoC_B and energy consumption. The LPF method has the lowest current in Table 7 since it starts with the SoC condition of 95%. In the longer test, 4 times all phases, the SoC of SC in the second repetition is 80% and it cannot handle the peak power. As a result, the LPF peak battery current is higher than battery-only. Since its battery not only supplies the load but also charges the SC which is the power already used before peak load.

The weakness of both LPF and FLC is that both cannot predict the peak load power. Hence, the SC power is already used in the high load power event it is not the peak load power. The SC is already in the lower limit SoC when reaches the peak load. On the other hand, the

TABLE 4. Performance of WLTC-3a low-speed phase

Method	ΔSoC_B (%)	Energy consumption (kWh/km)	Max I_B (A)	BCRMS
Battery-only	1.10	0.061	109.33	26.89
LPF	1.13	0.063	65.12	16.65
FLC	1.13	0.062	110.62	24.82
LPF-ASL	1.13	0.063	65.12	16.64

TABLE 5. Performance of WLTC-3a medium-speed phase

Method	ΔSoC_B (%)	Energy consumption (kWh/km)	Max I_B (A)	BCRMS
Battery-only	2.30	0.083	144.73	49.79
LPF	2.03	0.074	103.03	36.81
FLC	2.04	0.074	134.27	46.32
LPF-ASL	2.05	0.074	136.85	37.69

TABLE 6. Performance of WLTC-3a high-speed phase

Method	ΔSoC_B (%)	Energy consumption (kWh/km)	Max I_B (A)	BCRMS
Battery-only	3.87	0.093	176.15	65.68
LPF	3.65	0.089	136.19	57.82
FLC	3.64	0.088	156.21	61.42
LPF-ASL	3.70	0.089	140.53	58.62

TABLE 7. Performance of WLTC-3a in all phases

Method	ΔSoC_B (%)	Energy consumption (kWh/km)	Max I_B (A)	BCRMS
Battery-only	7.26	0.083	176.19	47.78
LPF	6.81	0.079	138.37	38.94
FLC	6.77	0.078	178.03	45.11
LPF-ASL	6.85	0.079	140.40	39.24

TABLE 8. Performance of 4-times WLTC-3a in all phases

Method	ΔSoC_B (%)	Energy consumption (kWh/km)	Max I_B (A)	BCRMS
Battery-only	29.10	0.084	176.68	47.87
LPF	27.52	0.079	178.38	40.31
FLC	27.24	0.078	178.03	44.55
LPF-ASL	27.52	0.079	140.39	39.43

LPF-ASL, can adapt to the peak load based on the battery current and allocate some SC power for the peak load power. As a result, it can give the lowest peak battery current and BCRMS. Compared to the battery-only system, the HESS has a lower impact at low speeds and a higher impact at higher speeds. In the mixed speed phase and long-distance traveling, the HESS is superior to battery-only EVs. Since the main objective of this study is to minimize battery deterioration while ensuring efficient power distribution and the main criteria are battery peak current and BCRMS, the proposed LPF-ASL is superior to LPF and FLC.

The proposed method was then compared with the previous work with the same case study discussed by Maghfiroh et al. (48). They use optimal-LPF with static SoC limiter and tested in the Urban Dynamometer Driving Schedule (UDDS) with distances of 12,070 m (12 km). In this comparison, the same cut-off frequency and drive cycle are used which are 0.01Hz and UDDS, respectively. The difference is in the SoC limiter, where Maghfiroh et al. (48) used a static SoC limiter. The comparison results are shown in Table 9. The results show that from the two tests of UDDS, the pattern of all criteria is the same which is the proposed method has lower delta-SoCB, max I_B, and higher BCRMS. Whereas in terms of energy consumption, both tests give different results with only a bit difference. This test validates that the proposed method can effectively reduce the maximum battery current which is related to the battery stress.

TABLE 9. Comparison with reference (48)

Method	ΔSoC_B (%)	Energy consumption (kWh/km)	Max I_B (A)	BCRMS
1-times UDDS (12 km)				
LPF (48)	5.08	0.073	162.20	31.47
LPF-ASL	5.07	0.074	140.15	32.35
2-times UDDS (24 km)				
LPF (48)	10.20	0.075	162.50	31.85
LPF-ASL	10.18	0.074	140.54	32.45

3. 3. Power Distribution Analysis Figure 10 shows the power distribution from the EMS output before entering the SoC limiter. Figures 10(a) and 10(b) are from LPF EMS and FLC EMS, respectively. In the LPF EMS, the battery power reference is smooth since the high-frequency load power is sent to the SC. On the opposite, the battery power references from FLC EMS still contain high frequency, just reducing the peak power. As a result, the SC power is used more frequently in the LPF EMS. The power signal from EMS is then sent to the SoC limiter and converted to the current reference by dividing with DC-link voltage. There is only an SC current reference since the DC-DC converter is only on the SC side. The current reference signal for SC is depicted in Figure 11. Both limiters besides limiting the SoC usage also limit the reference current under ±100A which is the DC-DC converter limit. The LPF with a static limiter fluctuates more often than the adaptive one. This means it can not give current when peak load occurs since its SC SoC is already at the low limit due to current released at the high load which is not the peak load. The SC current from FLC EMS is low due to the determined rules. This pattern will change if the rules change.

Figures 12(a), 12(b), 12(c), and 12(d) show the power profiles of the battery-only, HESS LPF, HESS FLC, and HESS LPF-ASL, respectively, of the WLTC-3a all-phase test. Figure 12(a) makes it clear that the battery provides all of the load power. As opposed to the negative power, which recharges the battery while operating in the

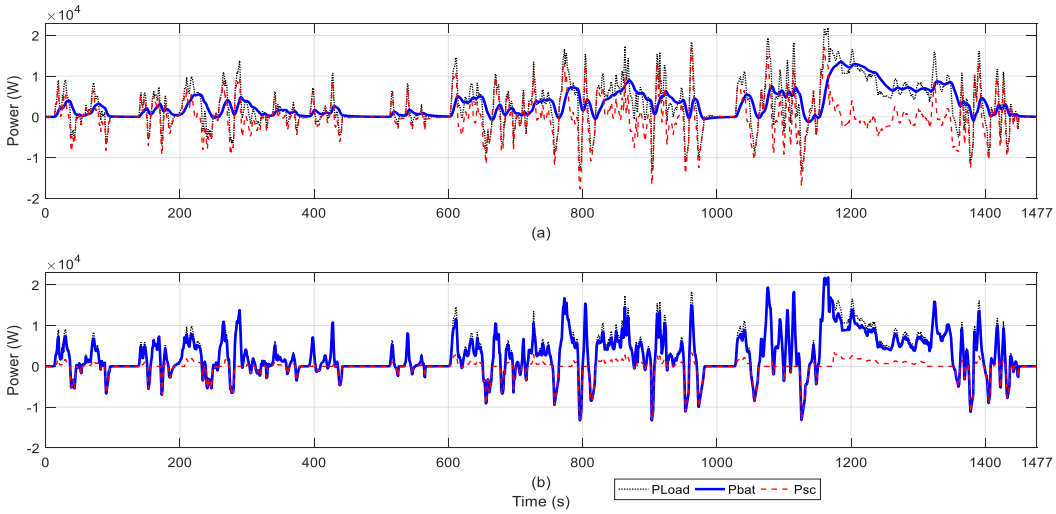

Figure 10. Power output from EMS without SoC limiter: (a) LPF EMS; (b) FLC EMS

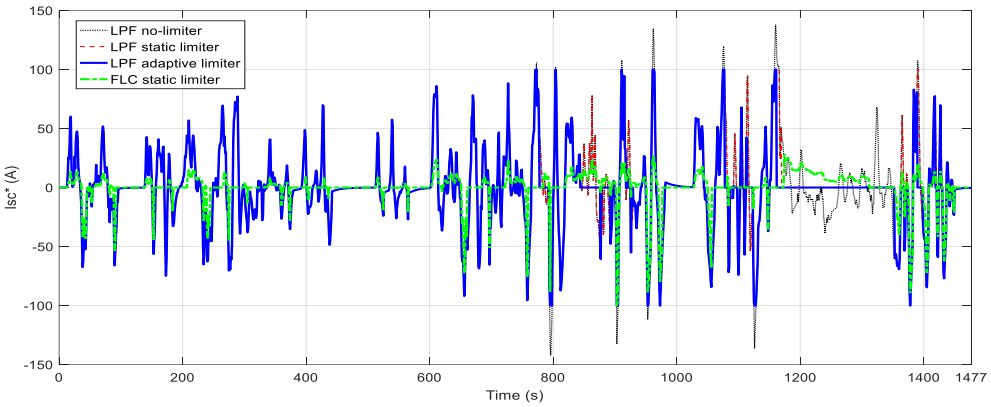

Figure 11. Current reference signal for SC

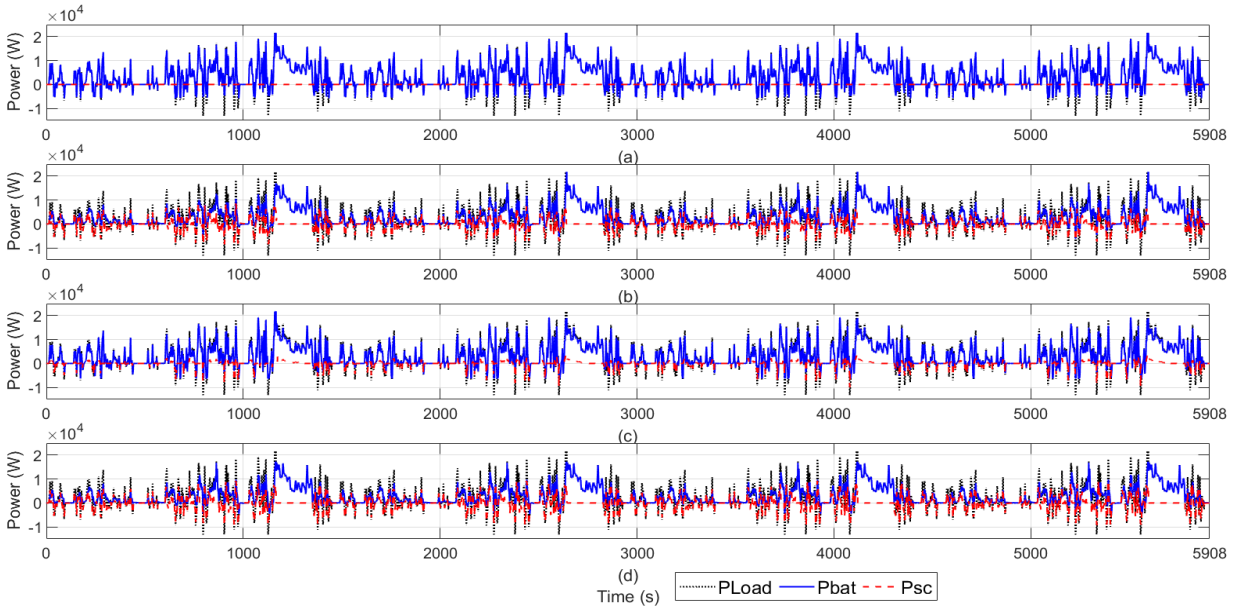

Figure 12. Power distribution: (a) battery-only; (b) HESS LPF; (c) HESS FLC

regenerative mode. Because the battery's charging current is limited in a battery-only system, the battery cannot absorb all of the regenerative power. Figures 12(b), 12(c), and 12(d) all make use of the supercapacitor. Positive power indicates that the battery and SC are supplied. Conversely, the negative power value signifies that it consumes the power generated by the regenerative braking. Since the HESS's current falls within the SC's current range, the regenerative power can be effectively collected by the SC. Because the battery and SC are connected via the DC bus, the charging process also takes place when one of them has a greater voltage. To stabilize the DC-link voltage, the higher voltage ESS will also charge the lower voltage ESS.

The difference between LPF EMS and FLC EMS is that in the LPF method, the charge and discharge of the battery and SC are more often. This is due to the LPF method, the working principle is only decoupling the low and high frequency; therefore, this phenomenon happens naturally, the higher voltage ESS will charge the low voltage one when the DC-DC converter is activated. On the other hand, the same process in the FLC method only happens when load power is negative or breaking based on the fuzzy rules. The proposed LPF-ASL has nearly the same pattern as LPF except for the lower power contributed by the SC. However, at the peak load power, it can give more SC power than other methods proved with the smallest peak battery current.

The battery and SC SoC changes in the HESS of the WLTC-3a test are shown in Figure 13. The HESS with FLC EMS has the highest battery SoC at the final point, as is seen in Figure 13(a). The LPF and LPF-ASL

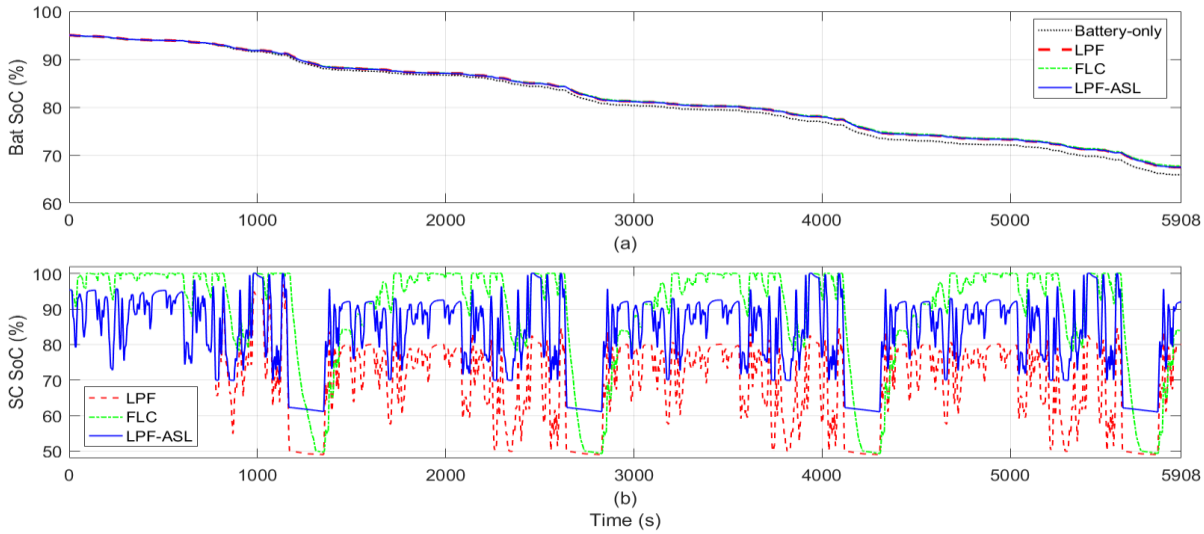

Figure 13. SoC: (a) battery SoC, (b) SC SoC

approaches are better than battery-only systems but worse than FLC EMS. For the battery-only, LPF, FLC, and LPF-ASL methods, the ultimate battery SoC values are 65.90%, 67.48%, 67.76%, and 67.48%, respectively. The battery is depleted and supplies power to the system when the SoC graph decreases, and vice versa. Figure 13(b) depicts the SC SoC graph. It charges and discharges as its value increases and decreases, respectively. The three EMS used to give different SC SoC patterns. The LPF with the static SoC limiter of 50-100% can give more SC power at the beginning. However, the SC SoC cannot come back at the end of the first cycle, as a result, the next cycle cannot be the same. The LPF-ASL with adaptive SoC limiter, in the low load power, has narrow SoC SC which can be used. As a result, the SC contribution in this EMS is lower than LPF but with a more stable SoC for all the cycles. The last, FLC, since it uses a lot of rules, only uses small SC power in the low load power (depending on the fuzzy rules). However, it can give higher power in the high load power condition. For the LPF, FLC, and LPF-ASL methods, the ultimate values of SC SoC are 80.04%, 83.85%, and 92.00%, respectively. The final SC SoC of the proposed method is higher than others since, in the peak current its SoC only decreases to 60%, whereas the others up to 50%.

4. CONCLUSION

The LPF with Adaptive State of Charge Limiter (LPF-ASL) is proposed to enhance real-time energy management in response to the limitations of LPF EMS, specifically its static SoC limiter. LPF-ASL dynamically allocates power for peak load events, addressing issues with suboptimal power utilization observed in LPF EMS. In a comprehensive PIL simulation considering delta-SoC, energy consumption, maximum battery current, and BCRMS, LPF-ASL demonstrates notable advantages. LPF EMS excels in reducing maximum battery current and BCRMS compared to FLC, while FLC outperforms LPF EMS in terms of delta-SoC and energy consumption. Significantly, in an unpredictable initial SC SoC test, LPF-ASL achieves substantial reductions in maximum battery current compared to LPF and FLC (up to 21.30% and 21.14%, respectively). This positions LPF-ASL as a promising solution for peak load handling in Hybrid Energy Storage Systems for Electric Vehicles. Looking forward, future studies could explore optimizing the LPF cut-off frequency using an optimization algorithm. This advancement has the potential to further enhance the practical applicability and scientific value of LPF-ASL for ideal energy management.

5. REFERENCES

1. Bedewy BAH, Al-Timimy SRA. Estimate suitable location of solar power plants distribution by GIS spatial analysis. Civil Engineering Journal. 2023;9(5):1217-29. https://doi.org/10.28991/CEJ-2023-09-05-013
2. Ihsan B, Hamdani D, Hariyanto N. Pengaruh Strategi Pengisian Daya Terhadap Kenaikan Beban Puncak Akibat Penetrasi Kendaraan Listrik. Jurnal Nasional Teknik Elektro dan Teknologi Informasi. 2020;9(3):311-8. https://doi.org/10.22146/.v9i3.363
3. Sadeq T, Wai CK, Morris E, Tarbosh QA, Aydoğdu Ö. Optimal control strategy to maximize the performance of hybrid energy storage system for electric vehicle considering topography information. IEEE Access. 2020;8:216994-7007. https://doi.org/10.1109/ACCESS.2020.3040869

4. Günther S, Weber L, Bensmann AL, Hanke-Rauschenbach R. Structured analysis and review of filter-based control strategies for hybrid energy storage systems. IEEE Access. 2022;10:126269-84. https://doi.org/10.1109/ACCESS.2022.3226261
5. Hemmati R, Saboori H. Emergence of hybrid energy storage systems in renewable energy and transport applications–A review. Renewable and Sustainable Energy Reviews. 2016;65:11-23. http://doi.org/10.1016/j.rser.2016.06.029
6. Tarassodi P, Adabi J, Rezanejad M. Energy Management of an Integrated PV/Battery/Electric Vehicles Energy System Interfaced by a Multi-port Converter. International Journal of Engineering. 2023;36(8):1520-31. https://doi.org/10.5829/ije.2023.36.08b.12
7. Mohammadian M, Rouholamini M. Grid-price-dependent energy management of a building supplied by a multisource system integrated with hydrogen. International Journal of Engineering. 2016;29(1):40-8. https://doi.org/10.5829/idosi.ije.2016.29.01a.06
8. Saadat Foumani M, Delkhosh M. Modification of equivalent consumption minimization strategy for a hybrid electric vehicle. International Journal of Engineering, Transactions C: Aspects,. 2016;29(12):1757-64. https://doi.org/10.5829/idosi.ije.2016.29.12c.15
9. Tran D-D, Vafaeipour M, El Baghdadi M, Barrero R, Van Mierlo J, Hegazy O. Thorough state-of-the-art analysis of electric and hybrid vehicle powertrains: Topologies and integrated energy management strategies. Renewable and Sustainable Energy Reviews. 2020;119:109596. https://doi.org/10.1016/j.rser.2019.109596
10. Gautam AK, Tariq M, Pandey JP, Verma KS, Urooj S. Hybrid sources powered electric vehicle configuration and integrated optimal power management strategy. IEEE Access. 2022;10:121684-711. https://doi.org/10.1109/ACCESS.2022.3217771
11. Ehsani M, Singh KV, Bansal HO, Mehrjardi RT. State of the art and trends in electric and hybrid electric vehicles. Proceedings of the IEEE. 2021;109(6):967-84. https://doi.org/10.1109/JPROC.2021.3072788
12. Mohammed AS, Atnaw SM, Salau AO, Eneh JN. Review of optimal sizing and power management strategies for fuel cell/battery/super capacitor hybrid electric vehicles. Energy Reports. 2023;9:2213-28. https://doi.org/10.1016/j.egyr.2023.01.042
13. Xu N, Kong Y, Chu L, Ju H, Yang Z, Xu Z, et al. Towards a smarter energy management system for hybrid vehicles: A comprehensive review of control strategies. Applied Sciences. 2019;9(10):2026. https://doi.org/10.3390/app9102026
14. Teng T, Zhang X, Dong H, Xue Q. A comprehensive review of energy management optimization strategies for fuel cell passenger vehicle. International Journal of Hydrogen Energy. 2020;45(39):20293-303. https://doi.org/10.1016/j.ijhydene.2019.12.202
15. Delkhosh M, Saadat Foumani M, Lashgarian Azad N. A New Framework for Advancement of Power Management Strategies in Hybrid Electric Vehicles. International Journal of Engineering, Transactions C: Aspects,. 2020;33(3):468-76. https://doi.org/10.5829/ije.2020.33.03c.11
16. Asensio EM, Magallan GA, De Angelo CH, Serra FM. Energy management on battery/ultracapacitor hybrid energy storage system based on adjustable bandwidth filter and sliding-mode control. Journal of Energy Storage. 2020;30:101569. https://doi.org/10.1016/j.est.2020.101569
17. Jiao Y, Månsson D. A study of the energy exchange within a hybrid energy storage system and a comparison of the capacities, lifetimes, and costs of different systems. Energies. 2021;14(21):7045. https://doi.org/10.3390/en14217045
18. Ramos GA, Costa-Castelló R. Energy management strategies for hybrid energy storage systems based on filter control: Analysis and comparison. Electronics. 2022;11(10):1631. https://doi.org/10.3390/electronics11101631
19. Tao F, Zhu L, Fu Z, Si P, Sun L. Frequency decoupling-based energy management strategy for fuel cell/battery/ultracapacitor hybrid vehicle using fuzzy control method. IEEE Access. 2020;8:166491-502. https://doi.org/10.1109/ACCESS.2020.3023470
20. Traoré B, Doumiati M, Morel C, Olivier J-C, Soumaoro O, editors. New energy management algorithm based on filtering for electrical losses minimization in Battery-Ultracapacitor electric vehicles. 2020 22nd European Conference on Power Electronics and Applications (EPE'20 ECCE Europe); 2020: IEEE.
21. Snoussi J, Ben Elghali S, Benbouzid M, Mimouni MF. Auto-adaptive filtering-based energy management strategy for fuel cell hybrid electric vehicles. Energies. 2018;11(8):2118. https://doi.org/10.3390/en11082118
22. Maghfiroh H, Wahyunggoro O, Cahyadi AI. Optimizing Low Pass Filter Cut-off Frequency for Energy Management in Electric Vehicles with Hybrid Energy Storage Systems. Mathematical Modelling of Engineering Problems. 2023;10(5). https://doi.org/10.18280/mmep.100539
23. Dang QB, Dinh AV, Vo-Duy T, Ta MC, editors. An energy management system based on fuzzy-lpf for hess of electric vehicles. 2019 IEEE Vehicle Power and Propulsion Conference (VPPC); 2019: IEEE.
24. Dang QB, Ngoc ND, Phuong VH, Ta MC, editors. Implementation of frequency-approach-based energy management for EVs using typhoon HIL402. 2019 IEEE Vehicle Power and Propulsion Conference (VPPC); 2019: IEEE.
25. Salari O, Zaad KH, Bakhshai A, Jain P, editors. Filter design for energy management control of hybrid energy storage systems in electric vehicles. 2018 9th IEEE International Symposium on Power Electronics for Distributed Generation Systems (PEDG); 2018: IEEE.
26. Panda A, Mishra MK, editors. Power management of hybrid storage using rule based adaptive filtering in electric vehicle. 2022 IEEE International Conference on Power Electronics, Smart Grid, and Renewable Energy (PESGRE); 2022: IEEE.
27. Kimura R, Kondo K, Aiso K, Kobayashi H, Sakamoto S, Okada A, et al., editors. A Method to Design A Power Flow and Energy Management Controller for Battery and EDLC Hybrid Electric Vehicle. 2021 IEEE 30th International Symposium on Industrial Electronics (ISIE); 2021: IEEE.
28. Huang J, Huang Z, Wu Y, Liao H, Liu Y, Li H, et al., editors. Optimal filter-based energy management for hybrid energy storage systems with energy consumption minimization. 2020 IEEE International Conference on Systems, Man, and Cybernetics (SMC); 2020: IEEE.
29. El Aoumari A, Oaudi H, editors. Optimization of hybrid energy management for HTE vehicles. IECON 2021–47th Annual Conference of the IEEE Industrial Electronics Society; 2021: IEEE.
30. Zhang X, Lu Z, Tan C, Wang Z. Fuzzy Adaptive Filtering-Based Energy Management for Hybrid Energy Storage System. Computer Systems Science & Engineering. 2021;36(1). https://doi.org/10.32604/csse.2021.014081
31. Liao H, Peng J, Wu Y, Li H, Zhou Y, Zhang X, et al. Adaptive split-frequency quantitative power allocation for hybrid energy storage systems. IEEE Transactions on Transportation Electrification. 2021;7(4):2306-17. https://doi.org/10.1109/TTE.2021.3070849

32. Syahbana DF, Trilaksono BR, editors. MPC and filtering-based energy management in fuel cell/battery/supercapacitor hybrid source. 2019 International Conference on Electrical Engineering and Informatics (ICEEI); 2019: IEEE.
33. Snoussi J, Elghali SB, Mimouni MF, editors. Sizing and control of onboard multisource power system for electric vehicle. 2019 19th International Conference on Sciences and Techniques of Automatic Control and Computer Engineering (STA); 2019: IEEE.
34. Yi F, Lu D, Wang X, Pan C, Tao Y, Zhou J, et al. Energy management strategy for hybrid energy storage electric vehicles based on pontryagin's minimum principle considering battery degradation. Sustainability. 2022;14(3):1214. https://doi.org/10.3390/su14031214
35. Michalczuk M, Ufnalski B, Grzesiak LM. Fuzzy logic based power management strategy using topographic data for an electric vehicle with a battery-ultracapacitor energy storage. COMPEL: The International Journal for Computation and Mathematics in Electrical and Electronic Engineering. 2015;34(1):173-88. https://doi.org/10.1108/COMPEL-11-2013-0388
36. Onori S, Serrao L, Rizzoni G. Hybrid electric vehicles: Energy management strategies: Springer; 2016.
37. Tremblay O, Dessaint L-A. Experimental validation of a battery dynamic model for EV applications. World electric vehicle journal. 2009;3(2):289-98. https://doi.org/10.3390/wevj3020289
38. Miniguano H, Barrado A, Fernández C, Zumel P, Lázaro A. A general parameter identification procedure used for the comparative study of supercapacitors models. Energies. 2019;12(9):1776. https://doi.org/10.3390/en12091776
39. Hussain S, Ali MU, Park G-S, Nengroo SH, Khan MA, Kim H-J. A real-time bi-adaptive controller-based energy management system for battery–supercapacitor hybrid electric vehicles. Energies. 2019;12(24):4662. https://doi.org/10.3390/en12244662
40. Maghfiroh H, Hermanu C, Ibrahim MH, Anwar M, Ramelan A. Hybrid fuzzy-PID like optimal control to reduce energy consumption. TELKOMNIKA (Telecommunication Computing Electronics and Control). 2020;18(4):2053-61. http://doi.org/10.12928/telkomnika.v18i4.14535
41. Lin C, Luo W, Lan H, Hu C. Research on Multi-Objective Compound Energy Management Strategy Based on Fuzzy Control for FCHEV. Energies. 2022;15(5):1721. https://doi.org/10.3390/en15051721
42. Najjaran S, Rahmani Z, Hassanzadeh M. Fuzzy predictive control strategy for plug-in hybrid electric vehicles over multiple driving cycles. International Journal of Dynamics and Control. 2022;10(3):930-41. https://doi.org/10.1007/s40435-021-00862-9
43. Suhail M, Akhtar I, Kirmani S, Jameel M. Development of progressive fuzzy logic and ANFIS control for energy management of plug-in hybrid electric vehicle. Ieee Access. 2021;9:62219-31. https://doi.org/10.1109/ACCESS.2021.3073862
44. Krithika V, Subramani C. A comprehensive review on choice of hybrid vehicles and power converters, control strategies for hybrid electric vehicles. International journal of energy research. 2018;42(5):1789-812. https://doi.org/10.1002/er.3952
45. Geetha A, Subramani C. A comprehensive review on energy management strategies of hybrid energy storage system for electric vehicles. International Journal of Energy Research. 2017;41(13):1817-34. https://doi.org/10.1002/er
46. Huang Y, Wang H, Khajepour A, Li B, Ji J, Zhao K, et al. A review of power management strategies and component sizing methods for hybrid vehicles. Renewable and Sustainable Energy Reviews. 2018;96:132-44. https://doi.org/10.1016/j.rser.2018.07.020
47. DiselNet ETC. Worldwide harmonized light vehicles test cycle (WLTC). 2019.
48. Maghfiroh H, Wahyunggoro O, Cahyadi AI. Novel iterative Ragone plot-based optimization of low pass filter for hybrid power sources electric vehicles. e-Prime-Advances in Electrical Engineering, Electronics and Energy. 2024;7:100389. https://doi.org/10.1016/j.prime.2023.100389

Persian Abstract

چکیده

وسایل نقلیه الکتریکی (EVs) به یک راه حل حیاتی برای حمل و نقل محیطی تبدیل شده اند. با این حال، چالش های مربوط به عمر باتری و چگالی توان همچنان ادامه دارد. به دنبال بهبود عملکرد EV و مقرون به صرفه بودن، محققان از سیستم‌های ذخیره‌سازی انرژی هیبریدی (HESS) حمایت می‌کنند که سیستم‌های مختلف ذخیره‌سازی انرژی (ESS)را یکپارچه می‌کنند. یک استراتژی مدیریت انرژی کارآمد (EMS)برای توزیع بهینه نیرو در HESS بسیار مهم است. این مطالعه یک EMS بلادرنگ، ساده و کاربردی را با استفاده از فیلتر پایین گذر (LPF)معرفی می‌کند. با این حال، LPF فاقد کنترل وضعیت شارژ (SoC)است که نیاز به افزودن یک محدود کننده SoC دارد. محدودکننده SoC استاتیک، در حالی که موثر است، در پیش‌بینی بارهای اوج با چالش‌هایی مواجه است که منجر به عملکرد تقسیم توان کمتر از حد مطلوب می‌شود. برای رفع این محدودیت، LPF با محدود کننده SoC تطبیقی (LPF-ASL)پیشنهاد شده است. LPF-ASL با صرفه جویی در بخشی از قدرت ابرخازن (SC)برای بار اوج، اوج بار را در خود جای می دهد. در یک آزمایش غیر قابل پیش بینی اولیه SC SoC، LPF-ASL به کاهش قابل توجهی در حداکثر جریان باتری در مقایسه با LPF و کنترل منطق فازی (FLC)تا ۲۱.۳۰٪ و ۲۱.۱۴٪ دست می یابد. این امر بر اثربخشی LPF-ASL در بهینه‌سازی عمر باتری و افزایش توزیع نیرو در خودروهای الکتریکی مجهز به HESS تاکید می‌کند.